Engineering xxx (xxxx) xxx

Contents lists available at ScienceDirect

Engineering

journal homepage: www.elsevier.com/locate/eng

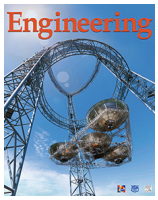

Article

Physics-Informed Deep Learning-Based Real-Time Structural Response Prediction Method

Ying Zhou *, Shiqiao Meng, Yujie Lou, Qingzhao Kong

State Key Laboratory of Disaster Reduction in Civil Engineering, Tongji University, Shanghai 200092, China

ARTICLE INFO

Article history:
Available online xxxx

Keywords:
Structural seismic response prediction
Physics information informed
Real-time prediction
Earthquake engineering
Data-driven machine learning

ABSTRACT

High-precision and efficient structural response prediction is essential for intelligent disaster prevention and mitigation in building structures, including post-earthquake damage assessment, structural health monitoring, and seismic resilience assessment of buildings. To improve the accuracy and efficiency of structural response prediction, this study proposes a novel physics-informed deep-learning-based real-time structural response prediction method that can predict a large number of nodes in a structure through a data-driven training method and an autoregressive training strategy. The proposed method includes a Phy-Seisformer model that incorporates the physical information of the structure into the model, thereby enabling higher-precision predictions. Experiments were conducted on a four-story masonry structure, an eleven-story reinforced concrete irregular structure, and a twenty-one-story reinforced concrete frame structure to verify the accuracy and efficiency of the proposed method. In addition, the effectiveness of the structure in the Phy-Seisformer model was verified using an ablation study. Furthermore, by conducting a comparative experiment, the impact of the range of seismic wave amplitudes on the prediction accuracy was studied. The experimental results show that the method proposed in this paper can achieve very high accuracy and at least 5000 times faster calculation speed than finite element calculations for different types of building structures.

© 2023 The Authors. Published by Elsevier LTD on behalf of Chinese Academy of Engineering and Higher Education Press Limited Compan. This is an open access article under the CC BY-NC-ND license (http://creativecommons.org/licenses/by-nc-nd/4.0/).

1. Introduction

High-precision and efficient structural response prediction is essential for intelligent disaster prevention and mitigation in building structures, including post-earthquake damage assessment, structural health monitoring, resilience assessment of buildings, and other aspects [1]. One of the core aspects of intelligent disaster prevention and mitigation in building structures is the intelligent assessment of structural damage [2], which can be realized by predicting and analyzing the response of structures under external loads. Therefore, high-precision and efficient real-time structural response prediction is essential in post-earthquake damage assessment, structural health monitoring, building seismic resilience assessment, and other applications.

Earthquakes are among the natural disasters that cause the largest losses of life and property worldwide. During major earthquakes, the damage and even collapse of buildings are the leading causes of economic losses and casualties [3]. When an earthquake disaster occurs, post-earthquake damage assessment of buildings in the earthquake area can provide critical decision-making information for rescuing the wounded and post-earthquake building repairs [4]. An essential aspect of the existing damage assessment methods is the simulation of earthquake disasters using numerical calculations [5,6]. This method uses the response information of building structures obtained through numerical calculations to calculate the degree of damage to building structures. In addition, the calculation of the response of a building structure under an earthquake can be used for structural health monitoring [7] and for assessing its seismic resilience [8] and vulnerability [9–11]. In summary, it is essential to predict the structural responses to earthquakes.

The current method for predicting the response of building structures to earthquakes with high precision is primarily based on finite-element time-history analysis [12]. This method has problems such as long computation time and a complex analysis process; therefore, real-time calculation of the structural response cannot be realized, which is unfavorable for rapid damage assessment and rescue after disasters. Supercomputers provide possible solutions [13]; however, the lack of openness of these computing resources currently limits their widespread use.

* Corresponding author.
E-mail address: yingzhou@tongji.edu.cn (Y. Zhou).

https://doi.org/10.1016/j.eng.2023.08.011
2095-8099/© 2023 The Authors. Published by Elsevier LTD on behalf of Chinese Academy of Engineering and Higher Education Press Limited Compan.
This is an open access article under the CC BY-NC-ND license (http://creativecommons.org/licenses/by-nc-nd/4.0/).

Please cite this article as: Y. Zhou, S. Meng, Y. Lou et al., Physics-Informed Deep Learning-Based Real-Time Structural Response Prediction Method, Engineering, https://doi.org/10.1016/j.eng.2023.08.011

To solve these problems, three main strategies are used in this research. The first strategy is to improve the time–history analysis method to solve the ground motion response, for example, by improving the input ground motion data preprocessing method, structure and component modeling method, and integration method [14–16]. Although this method can simplify the calculation of the time–history analysis to a certain extent, it cannot achieve real-time structural response calculations. The second strategy is to significantly reduce the computational complexity by establishing a simplified model that achieves an extremely fast but low-accuracy prediction of the overall structural response [17]. For example, Hori and Ichimura [18] simplified a building into a multi-degree-of-freedom system and realized real-time prediction of the overall response of the structure through a time–history analysis method. Lu and Guan [19] used an inter-story bending–shear model as a simplified model. The calculation of the building response is accelerated by the graphics processing unit (GPU); therefore, real-time prediction of the overall structural response can be realized at the city level. However, the models used in these methods are excessively simplified; therefore, the structural response can only be approximately calculated, making it challenging to achieve a refined damage assessment. In addition, because of the significant difference between the simplified model and the actual building, the prediction accuracy of the response is relatively low.

The last strategy involves approximating the seismic response of structures in a data-driven manner using machine learning methods, thereby avoiding the complex iterative integration process in the time–history analysis. Lin et al. [20] considered parameters such as building structure height and natural vibration period and used a support vector machine (SVM) to predict the peak acceleration of the floor. Oh et al. [21] used five parameters, including the average period of earthquake vibration and ground peak acceleration, as the input of a multilayer perceptron (MLP) and predicted the structure's maximum displacement and maximum inter-story displacement ratio. Papadrakakis and Lagaros [22] proposed an artificial neural network model combined with a performance-based design process to predict nonlinear seismic responses of buildings. Yang et al. [23] addressed the multistep prediction of strong earthquake ground motion and the seismic response of single-degree-of-freedom systems with the support of an empirical mode decomposition and extreme learning machine. Sahoo and Chakraverty [24] proposed a functionally linked neural network to predict the seismic responses of tall shear buildings. Tezcan and Marin-Artieda [25] proposed a least-squares SVM approach to estimate displacements from measured accelerations.

With the rapid development of deep learning, an increasing number of deep learning-based models with strong fitting abilities have been proposed, such as convolutional neural networks (CNNs) [26], recurrent neural networks [27], long short-term memory (LSTM) networks [28], and transformers [29]. Kim et al. [30] predicted the peak transient response of a nonlinear hysteresis system using a CNN. In another study by Kim et al. [31], a Bayesian deep learning approach was used, and the probability distribution of the peak displacements was provided. Some researchers focused on the time series of structural responses and conducted further evaluation analyses using sufficient sequence information. Wu and Jahanshahi [32] studied the problem of structural dynamic response estimation and system identification for building structures with multiple degrees of freedom using CNN models. Gao and Zhang [33] achieved structural response prediction using an LSTM network. Zhang et al. [34] proposed an LSTM network for predicting nonlinear structural seismic responses. Zhang et al. [35] proposed a physics-guided CNN model to provide data-driven seismic response predictions. The prediction results were within a 10% confidence interval compared with the actual structural vibration response, with a confidence level of more than 88%. Perez-Ramirez et al. [36] proposed a recurrent neural network with Bayesian training and mutual information for the response prediction of large buildings. Peng et al. [37] used piecewise linear least squares, a forward connected neural network, and an LSTM network to predict the response time history of nodes using autoregressive methods. An experiment for structural response prediction was conducted on a six-story steel-frame model. Eshkevari et al. [38] proposed a DynNet network by constructing a recurrent neural cell that updates the state from the current time step to the next with neural connections, inspired by exact numerical differential equation solvers. This method was tested on a four-degree-of-freedom structure.

These methods can be used to predict the structural response time history. However, they can only predict the overall response time history of a few nodes or floors in a building structure and cannot achieve a more accurate damage assessment. In addition, the above studies did not consider the physical information of the structure, such as its dynamic characteristics. Instead, these methods use only a large amount of data or physical laws to perform data-driven fitting. Finally, limited by the fitting ability of the data-driven model, most current research focuses only on the response prediction of single-story structures or simplified multi-story buildings, rather than the more complex response prediction of high-rise buildings.

To solve these problems, this study proposes a real-time prediction method for the structural response of a large number of nodes under seismic actions, combined with structural physical information. The dynamic characteristics of the building structure and other inherent structural information are introduced into the real-time response prediction method. A large amount of data is generated through numerical calculations to predict the real-time structural response of tall buildings. In addition, this study proposes a Phy-Seisformer model based on deep learning that realizes high-precision, real-time structural response predictions under seismic action. The main innovations of this study are summarized as follows:

(1) A novel real-time structural response prediction method under seismic action is proposed, which can predict a large number of nodes in the structure. Despite the prediction speed is remarkably high, the accuracy aligns closely to the calculation result driven from the finite-element time–history analysis.

(2) A novel deep-learning approach that uses a physics estimator to integrate structural dynamic characteristic information, Phy-Seisformer, is presented. The proposed model achieved highly accurate predictions for various building types. By leveraging the physics estimator, we significantly reduced the complexity of model fitting, leading to better overall prediction results.

2. Methodology

2.1. Overall process

A flowchart of the real-time prediction method for the structural response time history based on deep learning and physical information proposed in this paper is shown in Fig. 1. First, a refined finite element (FE) model of the structure is established, and a large number of seismic waves are selected as inputs for the finite element elastic or elasto–plastic time–history analysis. The above method can be used to obtain the acceleration, velocity, and displacement response time histories of all nodes in a structure under seismic action. Owing to the high accuracy and

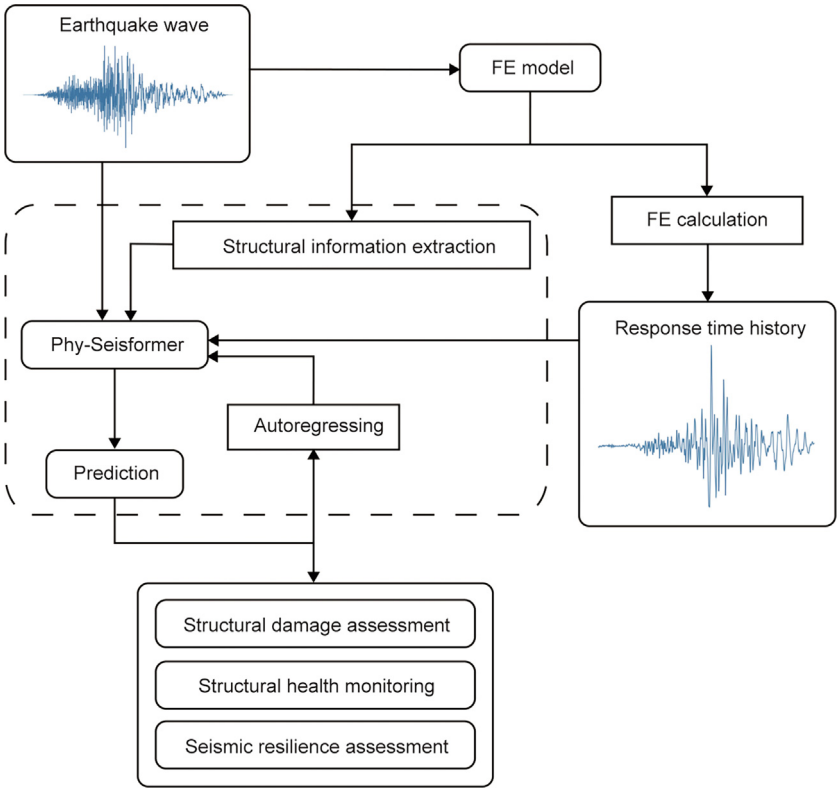

Fig. 1. Overall process of the physics-informed real-time structural response prediction method under seismic action. FE: finite element.

computational complexity of the refined FE model, high-precision structural response data can be obtained through massive numerical simulation calculations. Subsequently, in the structural dynamic information extraction module, the FE model of the building is simplified into a lumped mass model, in which each floor in the FE model is simplified into a mass point. After extracting the floor structure features of the simplified model, including the story mass and story stiffness, these features are inputted into the proposed Phy-Seisformer model. The last part is a real-time prediction model of the structural response time history based on deep learning, called Phy-Seisformer. The model input is the seismic wave and structural dynamic information, and the model output is the predicted response time history value of all nodes on the floor of the structure. Response prediction is achieved through an autoregressive mechanism. The model performs multiple autoregressive iterative calculations when dealing with complete seismic waves. Thus, the proposed method can predict the time history of a structural response under the action of seismic waves of any length. In the training phase of the Phy-Seisformer model, it is necessary to use the results of the FE calculations to create a dataset for model parameter optimization. In the model inference stage, only the seismic wave and structural dynamic information must be input to realize the rapid prediction of the structural response, which can be thousands of times faster than FE calculations. The results of the rapid prediction of the structural response can be used for the refined real-time assessment of building damage and other aspects.

The proposed physics-informed real-time structural response prediction method can effectively realize nonlinear structural response prediction, which is primarily realized in two aspects. First, the dataset for training the Phy-Seisformer model is calculated using nonlinear FE calculations; therefore, nonlinearity is inherent in the training dataset of the model. The second and more critical aspect is that the nonlinear stiffness information of the floors of the structure can be obtained through structural information extraction, which is then input into the Phy-Seisformer model. Based on the nonlinear stiffness information of the structure and through the physics estimator module in the Phy-Seisformer model, an elasto–plastic time–history analysis of the lumped mass model is performed. Thus, the model can process nonlinear structural information and perform response prediction.

2.2. Structural dynamic information extraction module

The primary function of the structural dynamic information extraction module proposed in this study was to extract the floor structure information required by the subsequent Phy-Seisformer model, including story mass and story stiffness. A schematic of the structural information extraction process is shown in Fig. 2. In this study, the seismic wave input was unidirectional. Therefore, it was only necessary to extract the story mass and stiffness of the FE model in the direction of the applied seismic waves.

The story mass is the sum of the masses of all the structural components and the floor's additional mass. The mass of the components connecting the upper and lower floors, such as the columns and walls, is evenly distributed between the upper and lower floors. The additional mass is the equivalent mass of the permanent and live loads, the specific values of which can be determined using the load code for the design of building structures [39].

The extraction of the story stiffness information is more complicated. The calculation method [40] using an empirical formula

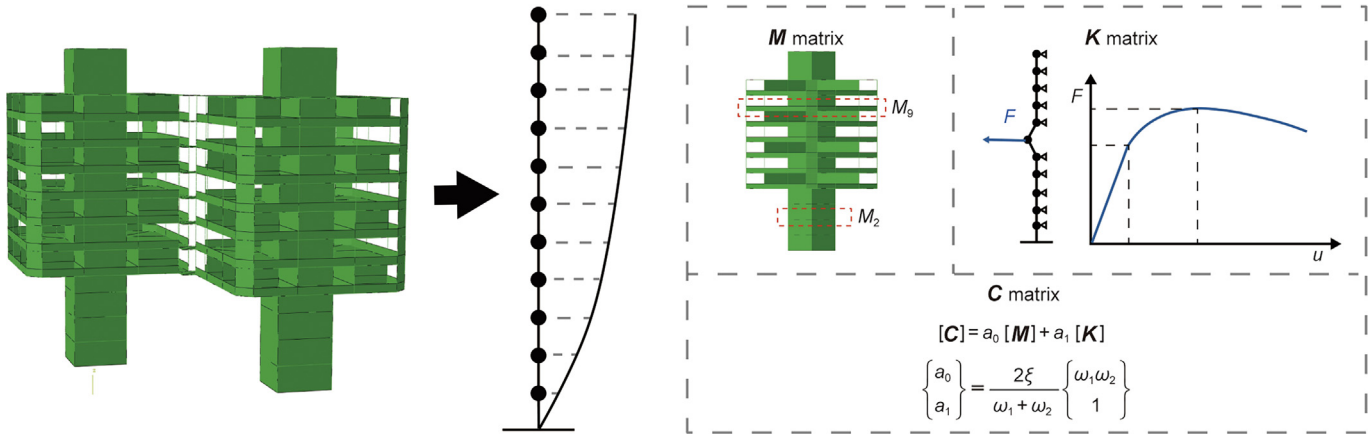

Fig. 2. Schematic of the structure information extraction module. ***C***: damping matrix; *a*: important parameter to calculate ***C***; *F*: force; *u*: displacement; ξ: damping ratio; ω_1 and ω_2: the structure's first- and second-order natural frequencies.

inevitably has a relatively large deviation and requires the use of different calculation methods for different structures, which is relatively complicated. As the FE model is known, a more accurate structural stiffness can be obtained through FE calculations. When calculating the stiffness of a specific story, it is necessary to fix the lateral displacement of all nodes in the upper and lower stories and apply a lateral force proportional to the mass at the specific story. The average displacement of all the nodes on the floor is calculated and considered as the story displacement. Subsequently, the lateral force is divided by the displacement to obtain the story stiffness curve. To bring the dynamic characteristics of the simplified model closer to those of the FE model, the first period of the simplified model and the main period of the FE model in the selected direction should be made equal by scaling the stiffness. The formula for this period is as follows:

$$T = 2\pi(\boldsymbol{MK}^{-1})^{1/2} \tag{1}$$

where T indicates the main period of FE model in the selected direction, $\boldsymbol{M}$ is the mass matrix, and $\boldsymbol{K}$ is the stiffness matrix. Therefore, the period of the simplified model and the FE model can be equalized by multiplying the overall stiffness of the simplified model by a coefficient f. The calculation formula of f is as follows:

$$S = (T/T')^2 \tag{2}$$

where S denotes the stiffness scaling factor of the simplified model, and T' is the first period of the simplified model.

2.3. Detailed structure of the Phy-Seisformer model

The Phy-Seisformer model proposed in this study includes a physics estimator module, two feature extraction modules, and a feature aggregation module. Among them, each module contains a SeisBlock module, which is mainly composed of multi-head self-attention mechanisms. Owing to the full consideration of structural dynamic information, which contains the story mass and story stiffness, the Phy-Seisformer can directly predict the response time history of all the nodes on a floor. The inputs of the physics estimator are the structural dynamic information and seismic wave, and its output is the predicted value of the floor response time history. The inputs to the two feature extraction modules are the seismic wave and physics estimator calculation results. Because the structural response is not only related to seismic waves but also to the historical response time history of the structure [37], the two feature extraction modules also need as input the response time history of the structure in multiple previous time steps. The input of the feature aggregation module in Phy-Seisformer is the output of the two feature extraction modules, and the output of the feature aggregation module is the predicted value of the response of the structural floor nodes. A detailed structural diagram of the Phy-Seisformer model is shown in Fig. 3.

The proposed Phy-Seisformer adopts an autoregressive prediction strategy to predict structural responses. The structural response prediction approach proposed in this study involves segment-wise iterative processing of the input seismic wave, instead of direct processing of the entire seismic wave. During each iterative prediction, the value of the structural response output predicted by the model serves as one of the input components for the subsequent model prediction. A schematic of the autoregressive prediction method used in this study is shown in Fig. 4. By fixing the length of the single input and output data in the time dimension of the model in the autoregressive process, the model's training process is simplified, and the structural response time history prediction for the seismic wave input of any length is realized. In addition, this method is not a pure autoregressive process, which relies on the historical structural response and uses the results of seismic waves and the physics estimator as inputs. Therefore, the impact of the iteration error on the prediction accuracy is significantly reduced. Finally, this method can significantly expand the number of samples in the training set and fully utilize a limited dataset for substantial data amplification. The remainder of this section introduces the various modules of the Phy-Seisformer model.

2.3.1. Physics estimator

In the physics estimator part of the model, the inputs of this module are structural dynamic information and seismic waves, and the output is an estimate of the overall response time history of the floor. Because the calculation process of this part utilizes the story mass and stiffness, and the structural dynamic equation is embedded, the physical information is fully considered in the calculation process instead of purely using data to fit the deep learning model. The proposed physics estimator module simplifies the complicated fitting problem of direct fitting from seismic waves to structural responses. This transforms the fitting problem of the seismic wave to any node in the structure into a fitting problem between the approximate and precise calculation results of the structural response. This simplification method dramatically reduces the complexity of the model in dealing with structural response prediction under seismic action and the difficulty of fitting the deep-learning-based model.

The specific calculation method involves a rapid calculation of the response prediction value of the floor using a simplified

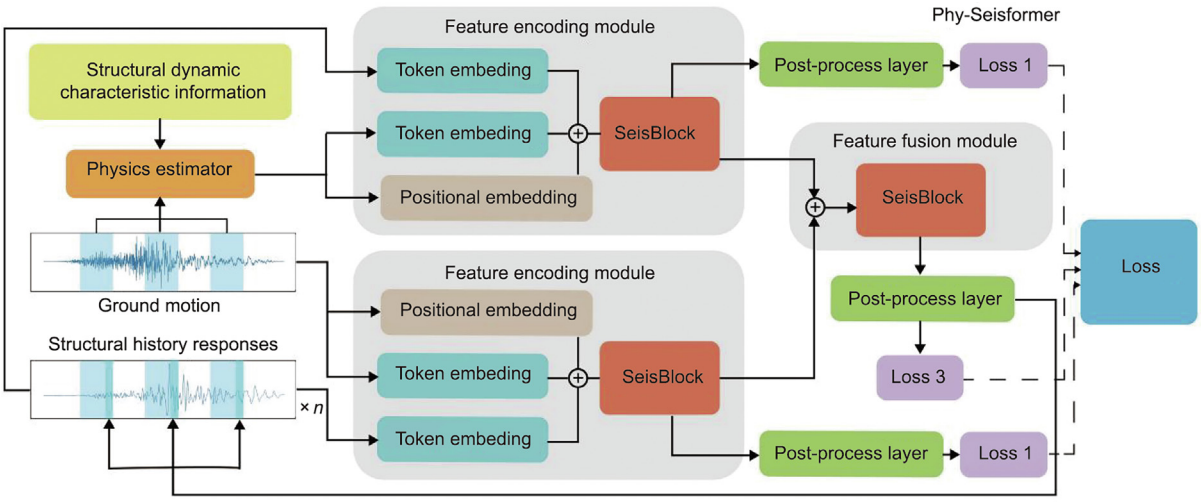

Fig. 3. Detailed structural diagram of the Phy-Seisformer model.

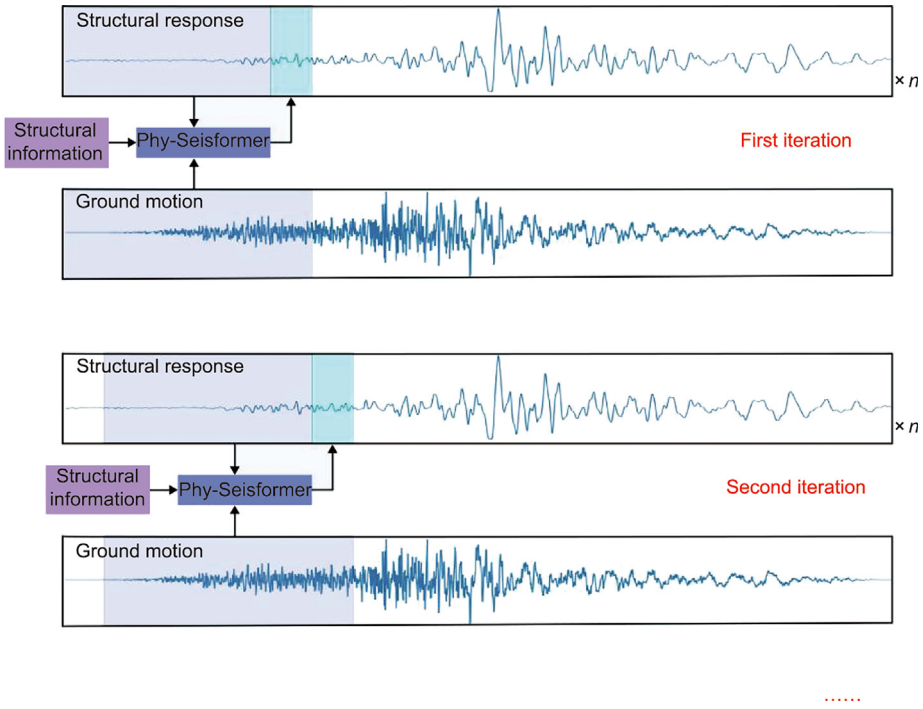

Fig. 4. Visualization of the autoregressive prediction method used in this study.

numerical calculation method and inputting it into the feature extraction module. The numerical calculation method can utilize any multi-degree-of-freedom structural response calculation method. This study used the Newmark-β method [41] for the calculation. The basic assumption of the Newmark-β method is that the acceleration changes linearly within the time interval $[t, t+\Delta t]$, and its expression is

$$\dot{u}_{t+\Delta t} = \dot{u}_t + [(1-\gamma)\ddot{u}_t + \gamma\ddot{u}_{t+\Delta t}]\Delta t \tag{3}$$

$$u_{t+\Delta t} = u_t + u_t\Delta t + [(1/2-\beta)\ddot{u}_t + \beta\ddot{u}_{t+\Delta t}]\Delta t^2 \tag{4}$$

where u, $\dot{u}$, and $\ddot{u}$ represent the floor displacement, velocity, and acceleration, respectively. γ and β are constants. Let $\boldsymbol{C}$ indicates the damping matrix, and $\boldsymbol{G}$ means the load vector. According to the structural dynamics equation, a structure must satisfy the following equation:

$$\boldsymbol{M}\ddot{u}_{t+\Delta t} + \boldsymbol{C}\dot{u}_{t+\Delta t} + \boldsymbol{K}u_{t+\Delta t} = \boldsymbol{G}_{t+\Delta t} \tag{5}$$

Substituting Eq. (3) and Eq. (4) into Eq. (5), the equation about $\ddot{u}_{t+\Delta t}$ can be obtained as

$$\hat{\boldsymbol{K}}u_{t+\Delta t} = \hat{\boldsymbol{G}}_{t+\Delta t} \tag{6}$$

where $\hat{K}$ and $\hat{R}_{t+\Delta t}$ can be expressed as follows:

$$\hat{\boldsymbol{K}} = \boldsymbol{K} + \frac{\gamma}{\beta\Delta t}\boldsymbol{C} + \frac{1}{\beta\Delta t^2}\boldsymbol{M} \tag{7}$$

$$\hat{\boldsymbol{G}}_{t+\Delta t} = \boldsymbol{G}_{t+\Delta t} + \boldsymbol{M}\left[\frac{1}{\beta\Delta t^2}u_t + \frac{1}{\beta\Delta t}\dot{u}_t + \left(\frac{1}{2\beta} - 1\right)\ddot{u}_t\right] + \boldsymbol{C}\left[\frac{\gamma}{\beta\Delta t}u_t + \left(\frac{\gamma}{\beta} - 1\right)\dot{u}_t + \left(\frac{\gamma}{2\beta} - 1\right)\Delta t\ddot{u}_t\right] \quad (8)$$

By solving Eq. (6), $u_{t+\Delta t}$ is obtained and introduced into Eqs. (3) and (4) to calculate $\dot{u}_{t+\Delta t}$ and $\ddot{u}_{t+\Delta t}$, respectively. Thus, an estimate of floor response is obtained. In this study, the damping matrix adopts Rayleigh damping [42], which is expressed as

$$\boldsymbol{C} = a_0\boldsymbol{M} + a_1\boldsymbol{K} \quad (9)$$

The calculation method for the two important parameters, a_0 and a_1 [42], is shown in Eq. (10).

$$\begin{Bmatrix} a_0 \\ a_1 \end{Bmatrix} = \frac{2\xi}{\omega_1 + \omega_2}\begin{Bmatrix} \omega_1\omega_2 \\ 1 \end{Bmatrix} \quad (10)$$

where ξ is the damping ratio. ω_1 and ω_2 are the structure's first- and second-order natural frequencies, respectively. Suppose that the FE model of the structure is elastic. In this case, the stiffness matrix of the simplified lumped mass model remains constant, and the damping matrix is also a constant value. However, when the FE model is an elasto–plastic model, the stiffness matrix varies as the floor displacement changes. The changing stiffness matrix can be calculated step by step through the story stiffness curve obtained in the structural dynamic information extraction module. By substituting it into the above equation, the approximate value of the structural response of the elasto–plastic model can be calculated.

2.3.2. Feature extraction module

In the feature extraction module proposed in this study, a token-embedding module is first used to preprocess and add the input features, which significantly increases the number of feature channels to 512 and plays a role in feature fusion. The token module is primarily implemented through a fully connected network or a one-dimensional CNN. The token-embedding module integrates both seismic ground motion and structural response history information as inputs. Positional embedding is used to preserve the temporal relationship between the input data [43]. The token module is expressed as Eq. (11).

$$D = \sum_{k=1}^{N}(\mathrm{MLP}(E_{t-i,k}, E_{t-i+1,k}, ..., E_{t,k}, E_{t+1,k}, ..., E_{t+j,k}) + \mathrm{MLP}(R_{t-i,k}, R_{t-i+1,k}, ..., R_{t-1,k})) + \mathrm{PE} \quad (11)$$

where D represents the output result of the token embedding module, t is the current time step, E denotes the ground motion data, R denotes the response time history data, N is the total number of nodes, PE indicates positional embedding [43], MLP indicates multilayer perceptron, and i and j represent the number of historical and predicted time steps, respectively. After completing data preprocessing, the SeisBlock module is employed based on the transformer model for encoding. The SeisBlock module, as depicted in Fig. 5, consists of two multi-head linear self-attention modules, a feed-forward module, multiple dropout layers, and layer-normalization layers. Additionally, a structural diagram of the multi-head linear self-attention module is presented in Fig. 5. The input features of SeisBlock are divided into eight equal parts based on the dimension of the channel dimension, and each sub-input has 64 channels, which are utilized as the query, key, and value for calculation, respectively, as shown in Eq. (12).

$$\boldsymbol{D}_i = \mathrm{softmax}\left(\frac{\boldsymbol{Q}\boldsymbol{W}_{Q,i}(\boldsymbol{L}_{K,i}\boldsymbol{K}\boldsymbol{W}_{K,i})}{\sqrt{d_k}}\right) * \boldsymbol{L}_{V,i}\boldsymbol{V}\boldsymbol{W}_{V,i} \quad (12)$$

where $\boldsymbol{P}$, $\boldsymbol{Q}$, and $\boldsymbol{V}$ represent the key, query, and value metrics, respectively, $\boldsymbol{L}$ is a fully connected layer in the projection layer, $\boldsymbol{W}_Q$ and $\boldsymbol{W}_V$ indicate the trainable weights in the multi-head linear self-attention module, $\boldsymbol{D}$ is the output of the linear self-attention module, and i represents one of the heads in the multi-head linear self-attention module. After obtaining the eight output features, all

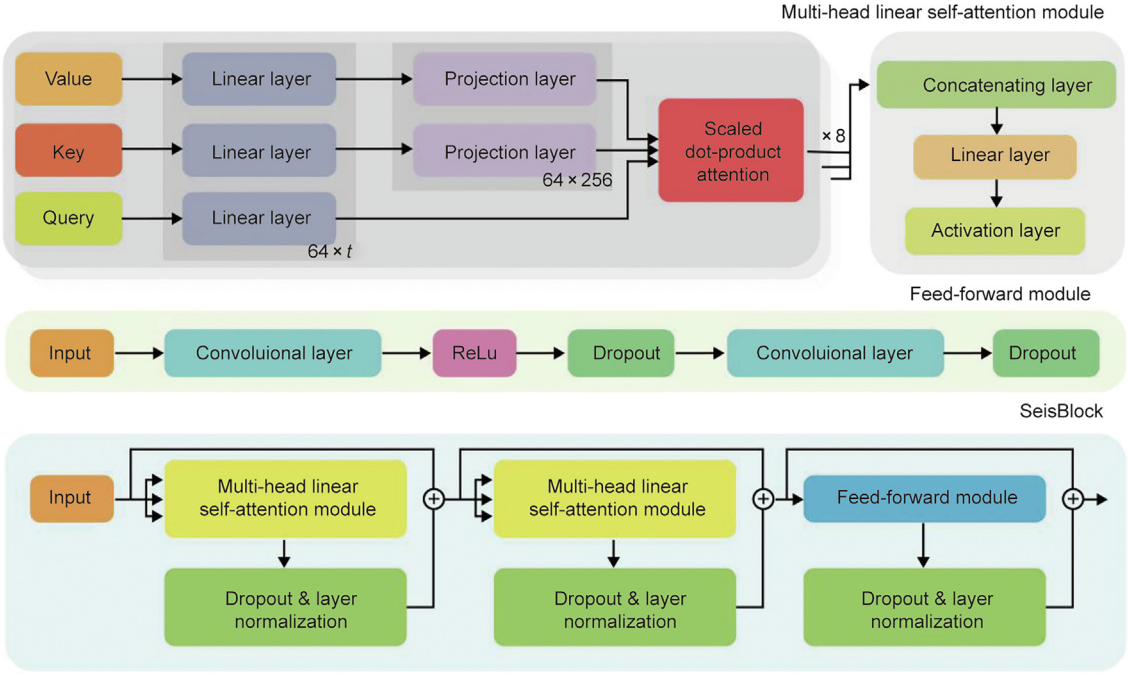

Fig. 5. Detailed structure of the SeisBlock module, the multi-head linear self-attention module, and the feed forward module. ReLu: rectified linear unit.

features are concatenated in the channel dimension and mapped through a linear layer to obtain the output result F, whose expression can be represented by Eq. (13).

$$F = W^F \begin{pmatrix} F_1 \\ F_2 \\ \cdots \\ F_8 \end{pmatrix} \tag{13}$$

where F represents the final output of the multi-head linear self-attention module, and $\boldsymbol{W_F}$ indicates the parameters of the linear layer. The network structure of the feed-forward module, as shown in Fig. 5, comprises two convolutional layers, two dropout layers, and a rectified linear unit [44].

Finally, the SeisBlock output is processed separately. This output is then fed into the subsequent feature aggregation module in the first aspect. However, through a fully connected layer, the encoded features are mapped to the dimensions of the response time history of all nodes, and the loss function is calculated in combination with the ground truth. It should be noted that the purpose of this operation is to obtain a better parameter training effect in the model training phase; therefore, the operation is performed solely during the training phase of the model and is not utilized during the inference phase.

2.3.3. Feature aggregation module

In the feature fusion module, the features extracted by the two feature extraction modules are first added and then calculated using the SeisBlock module. A fully connected layer is then employed to map the calculation results to each node to be predicted, and the response prediction value of multiple nodes on the same floor is obtained. In the model training phase, the results of the two feature extraction modules and feature aggregation modules must be processed by the fully connected layer. Subsequently, the loss function is calculated and added. In the reasoning stage of the model, the outputs of the feature aggregation module are used as the final prediction results.

3. Experiments of the structural response real-time prediction method

This section describes the dataset generation, model training, and model testing for multiple floors in a four-story masonry structure, an eleven-story reinforced concrete irregular structure, and a twenty-story reinforced concrete frame structure. To verify the effectiveness of the proposed method, elastic and elasto–plastic FE models were established for each building. Subsequently, the accuracy and efficiency of Phy-Seisformer in predicting the structural response time history of the elastic and elasto–plastic models were tested. The responses tested in the experiment were acceleration, velocity, and displacement. In addition, an ablation study was conducted to verify the effectiveness of the physics estimator in Phy-Seisformer. Furthermore, through a comparative experiment, the influence of the seismic wave amplitude range on prediction accuracy was studied.

3.1. Dataset generation and experiment details

3.1.1. Seismic wave selection

In this study, 200 seismic waves were selected, which were obtained from the Pacific Earthquake Engineering Research (PEER) Ground Motion Database and coded for the seismic design of buildings [45]. Considering that all the building structures utilized in the experiment are situated in Shanghai, China, our methodology for selecting suitable seismic waves references the response spectrum outlined in the "code for seismic design of buildings" of Shanghai [45]. The response spectrum for Shanghai is shown in Fig. 6. The expression for the response spectra is given by Eq. (14):

$$\alpha = \begin{cases} 0.45\alpha_{\max} + (10\eta_2 - 4.5)\alpha_{\max} T_n & T_n < 0.1 \\ \eta_2 \alpha_{\max} & 0.1 \le T_n < T_g \\ (T_g/T_n)^{\gamma}\eta_2\alpha_{\max} & T_g \le T_n < 5T_g \\ [\eta_2 0.2^{\gamma} - \eta_1(T - 5T_g)]\alpha_{\max} & 5T_g \le T_n < 6.0 \\ [\eta_2 0.2^{\gamma} - \eta_1(6 - 5T_g)]\alpha_{\max} & 6.0 \le T_n < 10.0 \end{cases} \tag{14}$$

where α is the seismic impact coefficient, α_{max} is the maximum value of the seismic impact coefficient, η_1 is the slope adjustment factor, η_2 is the damping modification factor, T_g is the feature period, and T_n is the natural vibration period. For minor and moderate earthquakes, the feature period was defined as 0.9 s; while for major earthquakes, it was set as 1.1 s. To select suitable seismic waves for experimentation, we utilized a specific method for computing the mean square error (MSE) between each seismic wave from the PEER database and the normed response spectrum outlined in the aforementioned code. Finally, we selected 186 seismic waves with the smallest MSE, along with 14 recommended seismic waves specified in the "code for seismic design of buildings" [45] to establish a dataset of 200 seismic waves for our experiment. Through this approach, we aimed to ensure that the selected seismic waves aligned with the characteristics of the Shanghai region and complied with the recommended seismic design practices. For the time–history analysis of the elastic model, the input seismic wave does not need to be amplitude modulated. In contrast, for the time–history analysis of the elasto–plastic model, the amplitude of the input seismic wave was adjusted to a random number in the range of 350–3500 mm·s^{-2}. The time interval for the seismic wave input was 0.02 s. In total, 140 seismic waves were randomly selected as the training set, 20 as the verification set, and 40 as the test set. Specific information regarding the selected seismic waves is provided in Table S1 in Appendix A.

3.1.2. Data augmentation

Because the Phy-Seisformer model proposed in this study performs iterative prediction, such as autoregressive prediction, and further expands the dataset to leverage the advantages of deep learning, this study augments the dataset by overlapping partitioning. In the training phase of the model, the structural history response input to Phy-Seisformer is the ground truth; therefore, each batch in the training set can be sampled overlappingly in the complete seismic wave sequence, rather than strictly following the autoregressive method in time order. An overlap-based data segmentation technique was utilized to generate training datasets for the Phy-Seisformer model. Specifically, we divided the sequence corresponding to a single seismic wave into thousands of time-series segments of equal length. The starting time steps of adjacent segments differed by only one time step. Using this

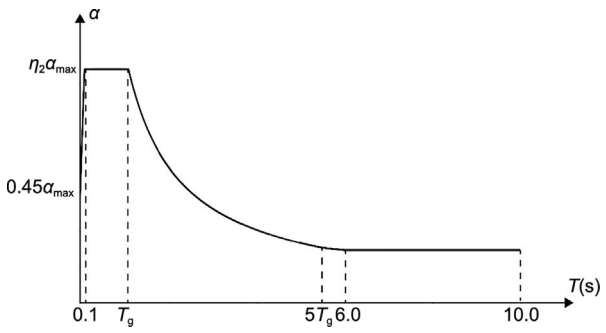

Fig. 6. Seismic impact coefficient curve of Shanghai.

overlap-based segmentation approach, we significantly expanded the limited seismic time series data and improved the training effectiveness of the Phy-Seisformer model. This operation can yield overlapping training data, thereby significantly increasing the number of datasets used for training. During the inference stage of the model, it is essential to input the seismic wave information step-by-step in chronological order.

3.1.3. Evaluation metrics

The evaluation metrics used in this experiment can be roughly divided into accuracy and speed. The mean absolute error (MAE), MSE, and Pearson coefficient (R) were selected as metrics to evaluate the prediction accuracy of the model. The calculation speed relative to that of the FE method measures the inference speed of the model. It should be noted that the specific values of MAE and MSE were related to the seismic amplitude in the experiment. The normalized seismic amplitude of this experiment was 3.5, which was restored to the original amplitude after processing by Phy-Seisformer. To establish a unified evaluation standard, the response time history corresponding to a seismic amplitude of 3.5 was used to calculate MAE and MSE rather than the response time history restored to the original amplitude. Addtionally, the values of all the evaluation metrics in the experiment were the average values of the 40 seismic waves in the test set. The metric definitions are given in Eqs. (15)–(18),

$$\mathrm{MAE} = \frac{1}{L_s}\sum_i |y_i - y_i'| \tag{15}$$

$$\mathrm{MSE} = \frac{1}{L_s}\sum_i (y_i - y_i')^2 \tag{16}$$

$$R = \frac{\sum_i \left(\mathrm{y}_i - \bar{y}\right)\left(\mathrm{y}_i' - \bar{y}'\right)}{\sqrt{\sum_i \left(\mathrm{y}_i - \bar{y}\right)^2}\sqrt{\sum_i \left(\mathrm{y}_i' - \bar{y}'\right)^2}} \tag{17}$$

$$\eta_r = \frac{t_s}{t_f} \tag{18}$$

where y_i and y_i' represent the predicted and actual values of the ith time step in the structural response time sequence, respectively. $\bar{y}$ and $\bar{y}'$ are the mean values of the predicted and actual values, respectively, of all the time steps in the structural response time sequence. L_s is the length of the entire sequence. η_r is the relative speed of the inference. t_s and t_f represent the time required to calculate the structural response under seismic action using Phy-Seisformer and FE time–history analysis, respectively.

3.1.4. Experiment details

In this study, all FE calculations were performed using Abaqus 2020. The implicit calculation method was employed, which requires an equilibrium iteration foreach incremental step of the simulation. If the balance condition is not satisfied within a particular incremental step, it is halved, and the calculation is repeated until convergence is achieved. The initial incremental step size is retained for subsequent calculations. If the incremental step size decreases to the minimum preset value, the computation is terminated. For this study, the initial incremental step size was set to 0.02 s, with a minimum incremental step of 1×10^{-8} s. These parameters were selected after considering the trade-off between computational accuracy and efficiency. The material properties of the building structure are elaborated in Sections 3.2 and 3.3.

The loss function used in this experiment was the MSE loss, and its expression is given by Eq. (19).

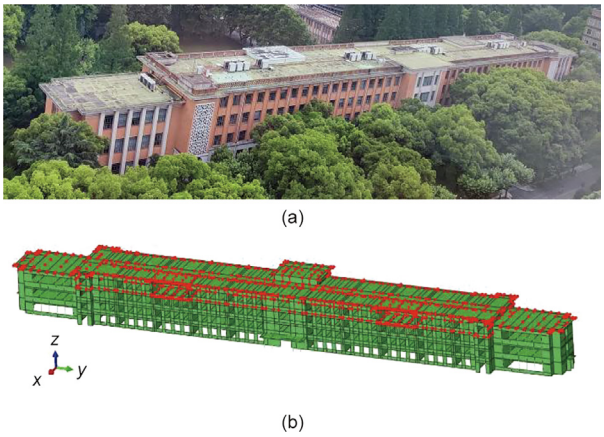

Fig. 7. Four-story masonry structure: (a) photograph and (b) the schematic of the FE model.

Table 1
Experimental results of the acceleration time history prediction for the elastic model of the four-story masonry structure.

Location	MAE	MSE	R	η_r
Floor 4	0.2414	0.4410	0.9697	8431.63
Roof	0.2538	0.7049	0.9803	8255.97

Table 2
Experimental results of the velocity time history prediction for the elastic model of the four-story masonry structure.

Location	MAE	MSE	R	η_r
Floor 4	0.1568	0.1533	0.9524	9646.70
Roof	0.2040	0.3222	0.9311	8446.00

Table 3
Experimental results of the displacement time history prediction for the elastic model of the four-story masonry structure.

Location	MAE	MSE	R	η_r
Floor 4	0.0830	0.0266	0.9924	9320.00
Roof	0.0439	0.0124	0.9970	8478.53

$$J = \frac{1}{N_d}\sum_{i=1}^{N_d}\sum_{j=1}^{N_t}\left[(y_{ij} - \hat{y}_{ij})^2 + (y_{ij}' - \hat{y}_{ij})^2 + (y_{ij}'' - \hat{y}_{ij})^2\right] \tag{19}$$

where J represents the loss function value, N_d indicates the batch size of training data, and N_t means the total number of time steps for a single prediction. y, y', and y'' represent the outputs of the feature aggregation module and two feature extraction modules, and ŷ is the ground truth. In this experiment, during the autoregressive process of the Phy-Seisformer model, the number of time steps for each input structure history response was 150, and the number of time steps for each prediction was 20. In the physics estimator, γ and β were 0.5 and 0.25, respectively.

It is essential to normalize the model input because the input of a single model is not a complete seismic wave, but a local seismic wave. Owing to the variations in the amplitudes of the seismic waves in the training set, the relationship between the seismic waves and structural responses can only be fitted with normaliza-

tion. The amplitude of all the seismic waves was input into the Phy-Seisformer model, as described in Section 3.5. The amplitude of the structural response was scaled using the same scaling ratio. It should be noted that these adjustments were made only during the calculation of the Phy-Seisformer model and not during the FE calculations. Furthermore, when Phy-Seisformer outputs the prediction results, they are divided by the previous scaling ratio to restore the actual response values. The Adam optimizer [46] was utilized for the experiment. The model training consisted of 100 epochs, with a learning rate of 0.00005. The FE calculations were all completed using Abaqus software, and the training of the Phy-Seisformer model was realized using Pytorch [47]. The experiment was conducted on an Intel (R) Xeon (R) Gold 6248 CPU @2.50 GHz, with an NVIDIA Telsa V100 GPU.

3.2. Structural response prediction experiments of the elastic model

3.2.1. Case 1: Elastic model of four-story masonry structure

This study conducted an experiment on a four-story masonry structure (Fig. 7(a)). The structure consists of brick masonry as the load-bearing construction material, with the story height of 3.85 m. In the FE model used for the experiment (Fig. 7(b)), the elastic modulus and Poisson's ratio of the brick masonry were set to 6304 MPa and 0.15, respectively. Additionally, the masonry structure included concrete structural columns and floor slabs. C25 concrete with a standard compressive strength of 25 MPa was selected for the concrete floors, while HPB300 steel bars with a standard value of yield strength at 3×10^5 kPa were used for the structure. Because the experiment employed an elastic FE model, only the linear phase of the material was considered as a material property. A damping ratio of 0.05 was adopted for the structure. The seismic waves were applied to the building in the *x*-direction because of its high vulnerability to seismic activity. All the nodes on the fourth floor and roof of the building, comprising 386 and 446 nodes, respectively, were selected for the experiment. The model was trained and tested for the acceleration, velocity, and displacement time histories of all the nodes on these floors. The response time histories considered in the experiment were absolute acceleration, absolute velocity, and absolute displacement. The detailed statistical results of the experiment are presented in Tables 1–3. Fig. 8 provides a visualization of the results, depicting the time history prediction results of the acceleration, velocity, and displacement of a node located at the top of the structure (roof) under the impact of the next generation attenuation (NGA)03806 seismic wave. The findings of the experiment demonstrated that the method proposed in this paper could deliver highly accurate response–time history predictions for masonry structures. Furthermore, the developed method exhibited a prediction speed was approximately 5000 times faster than that of the FE calculations.

3.2.2. Case 2: Elastic model of eleven-story reinforced concrete irregular structure

A schematic of the FE model of the eleven-story reinforced concrete irregular structure used in this test and a photograph of the structure are shown in Fig. 9. The height of each floor of the building was 3.9 m, and the construction materials included C20 concrete (with the standard value of compressive strength of 20 MPa) and HPB300 steel bars (with the standard value of yield strength of 3×10^5 kPa). As an elastic FE model was employed, only the linear phase of the material was considered. The elastic FE model yielded better simulation results for earthquakes with small amplitudes. The damping ratio of the structure was selected as 0.0605. All the seismic waves were applied in the *y*-direction, which is the most unfavorable direction for the seismic resistance of this building. All the nodes of the fourth floor, eighth floor, and roof were selected to perform the experiments, as indicated by the red markers in Fig. 9. This included eight nodes on the fourth floor, 50 nodes on the eighth floor, and 50 nodes on the top floor (roof). The acceleration, velocity, and displacement time histories were trained and predicted separately. The response time histories considered in the experiment were absolute acceleration, absolute velocity, and absolute displacement. Tables 4–6 list the statistical

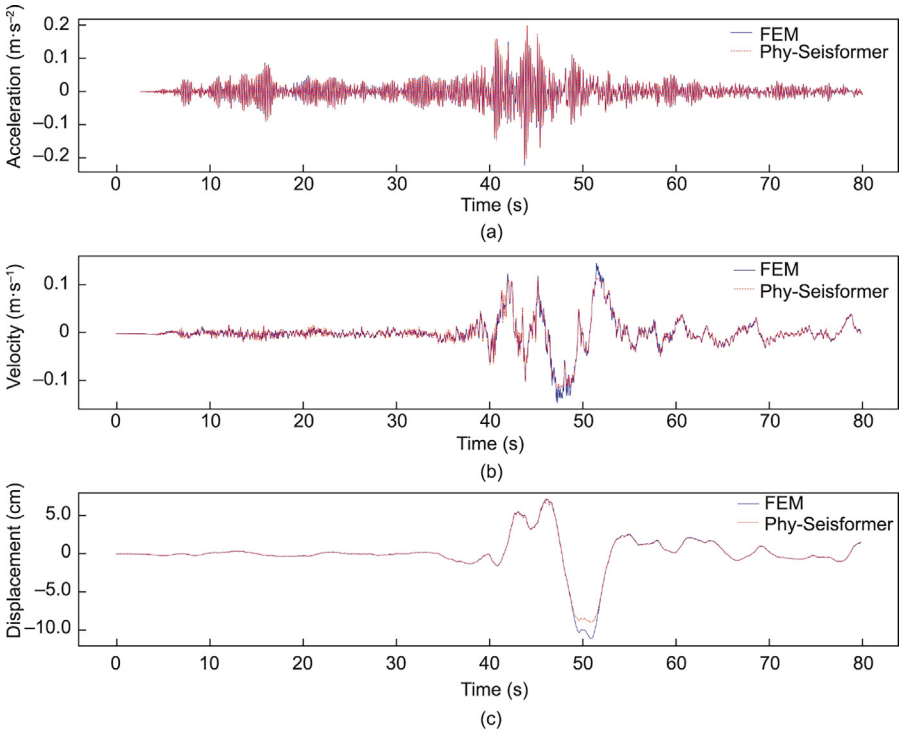

Fig. 8. Visualization of response time history prediction results of the elastic model of the four-story masonry structure. FEM: finite element method.

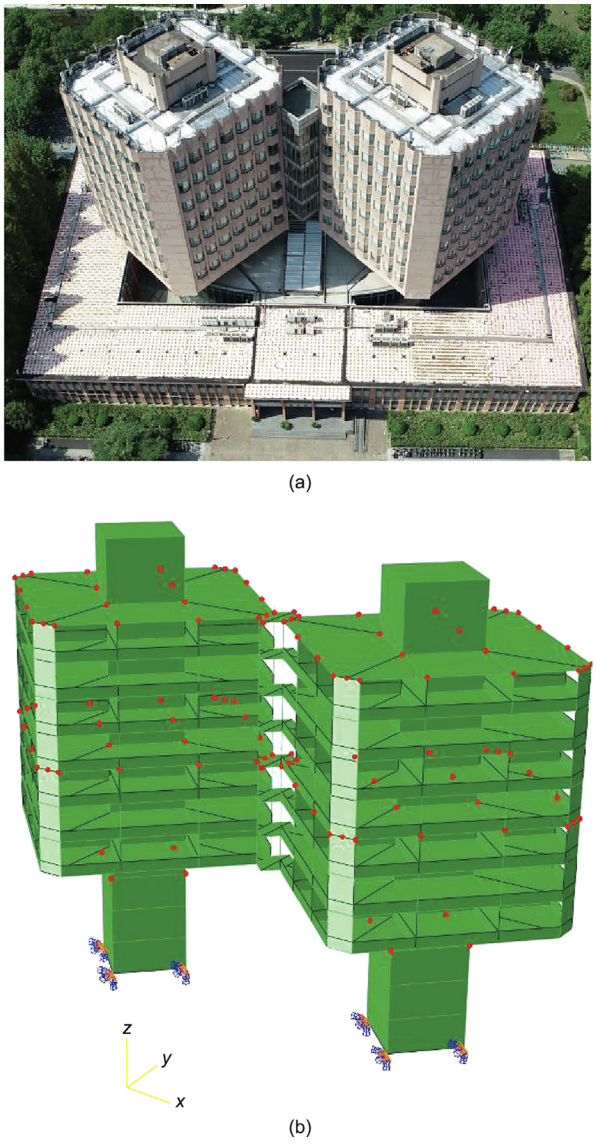

Fig. 9. Eleven-story reinforced concrete irregular structure: (a) photograph and (b) the schematic of the FE model.

values of the acceleration, velocity, and displacement response time histories for each floors. A visualization of the prediction results is presented in Fig. 10, which shows the time history prediction results of the acceleration, velocity, and displacement of a node on the top of the structure (roof) under the excitation of the NR1.1–6 seismic wave. The experimental results showed that the prediction of the Phy-Seisformer model closely matched the calculation results of the FE model, with a significantly higher calculation speed.

3.2.3. Case 3: Elastic model of twenty-one-story reinforced concrete frame structure

A schematic of the FE model and a photograph of the twenty-one-story reinforced concrete frame structure used in this experiment are shown in Fig. 11. The height of each floor of the building is 3.81 m, and the structure included a 2 m-high reinforcement layer formed by trusses every three floors. The overall height of the building is 98 m, with a plan size of 48.6 m × 48.6 m. The materials of the structure consists of C30 concrete (with the standard value of compressive strength of 30 MPa), C40 concrete (with the standard value of compressive strength of 40 MPa), and HPB300 steel bars (with the standard value of yield strength of 3×10^5 kPa). Similar to the previous experiment, an elastic FE model was employed, considering only the linear phase of the material. The damping ratio of the structure was selected as 0.0871. Because the *y*-direction is the most unfavorable direction for the seismic resistance of this building, all the seismic waves were applied in the *y*-direction. All the nodes on the fifth, tenth, fifteenth, twentieth, and roof floors were selected for the experiment, marked in red in Fig. 11, which include 71 nodes on the fifth floor, 151 nodes on the fifth floor, 73 nodes on the fifth floor, 73 nodes on the fifth floor, and 73 nodes on the top floor (roof). In addition, the training and prediction of the acceleration, velocity, and displacement time histories were performed separately. In this experiment, the acceleration response time history was relative to the ground, while the velocity and displacement response time histories were the absolute velocities and absolute displacement, respectively. Tables 7–9 list the statistical values of the acceleration, velocity, and displacement response time histories for each floor. Fig. 12 provides a visualization of the prediction results, displaying the time history prediction results of the acceleration, velocity, and displacement of a node on the top of the structure (roof) under the excitation of the NGA01817 seismic wave. The accuracy and efficiency of the Phy-Seisformer model in predicting the structural responses of high-rise buildings were verified.

Table 4
Experimental results of the acceleration time history prediction for the elastic model of the eleven-story irregular structure.

Location	MAE	MSE	*R*	η_T
Floor 4	0.0706	0.0259	0.9847	5639.79
Floor 8	0.0479	0.0104	0.9963	5737.40
Roof	0.0518	0.0156	0.9979	5552.64

Table 5
Experimental results of the velocity time history prediction for the elastic model of the eleven-story irregular structure.

Location	MAE	MSE	*R*	η_T
Floor 4	0.0969	0.0470	0.9739	5554.45
Floor 8	0.0990	0.0532	0.9880	5461.33
Roof	0.0712	0.0279	0.9957	5756.87

Table 6
Experimental results of the displacement time history prediction for the elastic model of the eleven-story irregular structure.

Location	MAE	MSE	*R*	η_T
Floor 4	0.0248	0.0015	0.9995	5939.40
Floor 8	0.0749	0.0134	0.9967	5564.88
Roof	0.0588	0.0100	0.9964	5323.79

3.3. Structural response prediction experiments of elasto–plastic model

3.3.1. Case 4: Elasto–plastic model of a four-story masonry structure

The four-story masonry structure utilized in this study was identical to the one employed in Section 3.2.1, except for the elasto–plastic materials used in this experiment. Nonlinear modeling was adopted to simulate concrete material behavior based on the specifications outlined in the "code for design of concrete structures" [48]. Figs. 13 and 14 show the compressive and tensile stress–strain curves of the concrete material and the bilinear isotropic hardening model used for the nonlinear modeling of the reinforcement. The complex nonlinear behavior of the masonry was modeled in the same manner as that described by Clementi [49]. The stress–strain constitutive relationships of the masonry

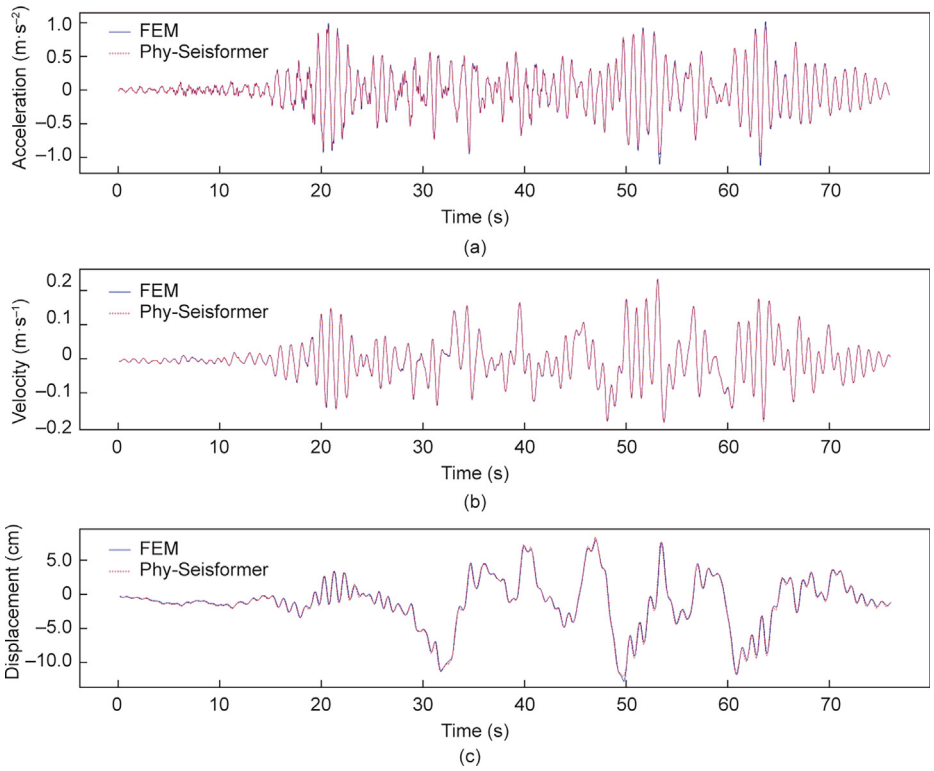

Fig. 10. Visualization of response time history prediction results of the elastic model of the eleven-story reinforced concrete irregular structure.

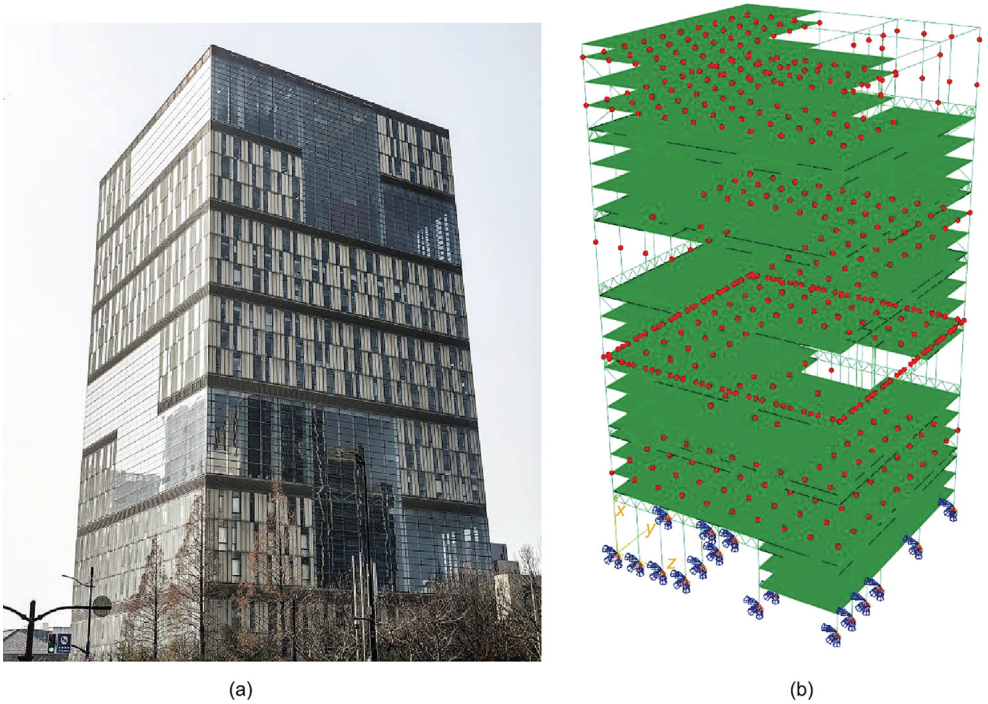

Fig. 11. Twenty-one-story reinforced concrete frame structure: (a) photograph and (b) the schematic of the FE model.

materials under uniaxial compression and uniaxial tension in the FE calculation are shown in Fig. 15. All the other test parameters were the same as those described in Section 3.2.1. Tables 10–12 list the statistical values of the acceleration, velocity, and displacement response time history predictions for each floor. Additionally, Fig. 16 illustrates the visualization of the predicted results, depicting the time history predictions of the acceleration, velocity, and displacement for a node at the top of the structure (roof) under the impact of the NGA01585 seismic wave. The experimental results verified that the proposed structural response prediction

Table 7
Experimental results of the acceleration time history prediction for the elastic model of the twenty-one-story reinforced concrete frame structure.

Location	MAE	MSE	*R*	η_r
Floor 5	0.1144	0.0572	0.9616	9670.59
Floor 10	0.1193	0.0539	0.9737	9912.78
Floor 15	0.1194	0.0478	0.9708	9318.69
Floor 20	0.0852	0.0281	0.9878	9491.70
Roof	0.0900	0.0346	0.9923	9367.77

Table 8
Experimental results of the velocity time history prediction for the elastic model of the twenty-one-story reinforced concrete frame structure.

Location	MAE	MSE	*R*	η_r
Floor 5	0.1556	0.0768	0.9551	10 004.39
Floor 10	0.0822	0.0239	0.9905	9 580.38
Floor 15	0.0993	0.0279	0.9940	9 488.10
Floor 20	0.0801	0.0225	0.9955	9 929.17
Roof	0.1543	0.0935	0.9865	9 483.48

Table 9
Experimental results of the displacement time history prediction for the elastic model of the twenty-one-story reinforced concrete frame structure.

Location	MAE	MSE	*R*	η_r
Floor 5	0.0485	0.0062	0.9974	10 026.70
Floor 10	0.1361	0.0322	0.9953	9 645.84
Floor 15	0.0766	0.0151	0.9966	9 882.80
Floor 20	0.1221	0.0395	0.9975	9 607.63
Roof	0.1375	0.0423	0.9956	9 381.10

method could deliver high prediction accuracy for masonry structures considering elasto–plastic modeling. Furthermore, as FE elasto–plastic calculation is notably more time-intensive than elastic calculations, the method proposed in this study is much faster in predicting the structural response of models using elasto–plastic materials compared to FE calculations.

3.3.2. Case 5: Elasto–plastic model of eleven-story reinforced concrete irregular structure

The eleven-story reinforced concrete irregular structure used in this experiment was the same building as described in Section 3.2.2, but with elasto–plastic materials instead of elastic ones. The nonlinear modeling approach for the concrete and steel reinforcement was identical to that described in Section 3.3.1. Except for the material properties, the other test parameters were the same as those in Section 3.2.2. Tables 13–15 list the statistical values of the acceleration, velocity, and displacement response time histories for each floor. A visualization of the prediction results is presented in Fig. 17, which shows the time history prediction results of the acceleration, velocity, and displacement of a node on the top of the structure (roof) under the excitation of the NGA01585 seismic wave. It can be observed from the experimental results that, compared to the prediction of the elastic FE model, the structural response prediction accuracy of Phy-Seisformer with the elasto–plastic model was lower. Nevertheless, the time history predictions of velocity and displacement achieved relatively similar results.

3.3.3. Case 6: Elasto–the plastic model of a twenty-one-story reinforced concrete frame structure

The twenty-two-story reinforced concrete frame structure used in this test was the same as described in Section 3.2.3. The nonlinear modeling of the materials in this building followed the same curves as those described in Section 3.3.1. Apart from the elasto–plastic materials, all other experimental parameters were the same as in Section 3.2.3. Tables 16–18 list the statistical values of the acceleration, velocity, and displacement response time histories for each floor. A visualization of the prediction results is presented in Fig. 18, which shows the time history prediction results of the acceleration, velocity, and displacement for a node on the top of

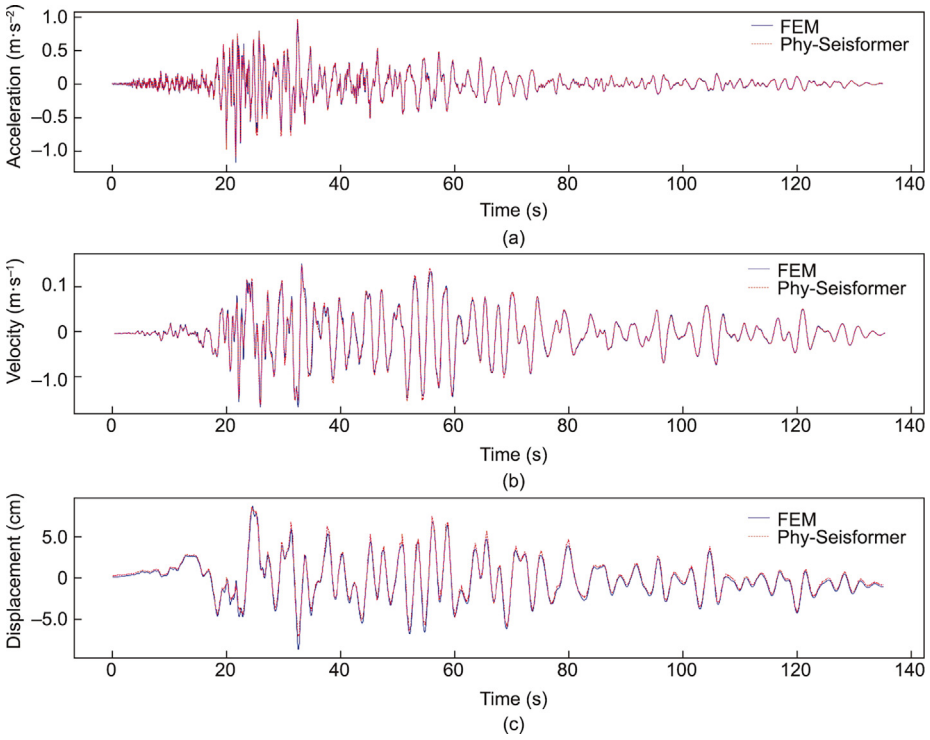

Fig. 12. Visualization of response time history prediction results for the elastic model of the twenty-one-story reinforced concrete frame structure.

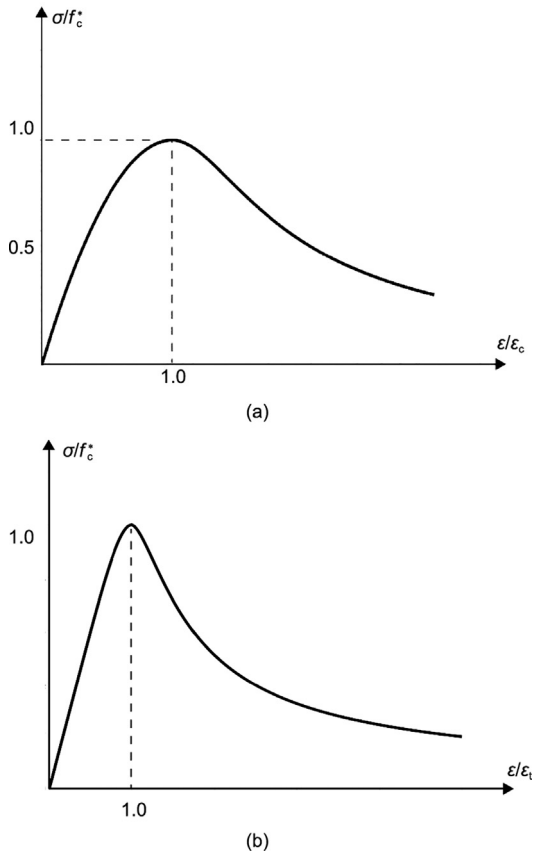

Fig. 13. Nonlinear modeling of concrete: (a) compressive behavior of concrete, where σ indicates the external stress, f_c^* is the uniaxial compressive strength of concrete, and ε_c is the peak strain corresponding to f_c^*; and (b) tensile behavior of concrete, where f_t^* is the uniaxial tensile strength of concrete, and ε_t is the peak strain corresponding to f_t^*.

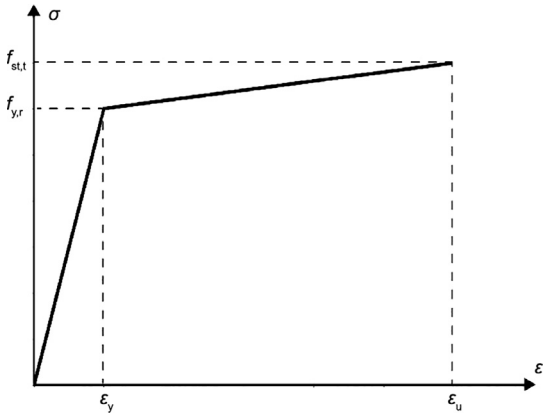

Fig. 14. Bilinear isotropic hardening model of the rebar, where $f_{y,r}$ is the yield strength of the rebar, ε_y is the yield strain corresponding to $f_{y,r}$, $f_{st,t}$ is the ultimate strength and ε_u is the ultimate strain corresponding to $f_{st,t}$.

the structure (roof) under the excitation of the NGA02074 seismic wave. The experimental results show that the proposed Phy-Seisformer can achieve high prediction accuracy and real-time prediction speed for super high-rise buildings using an elasto–plastic model dataset.

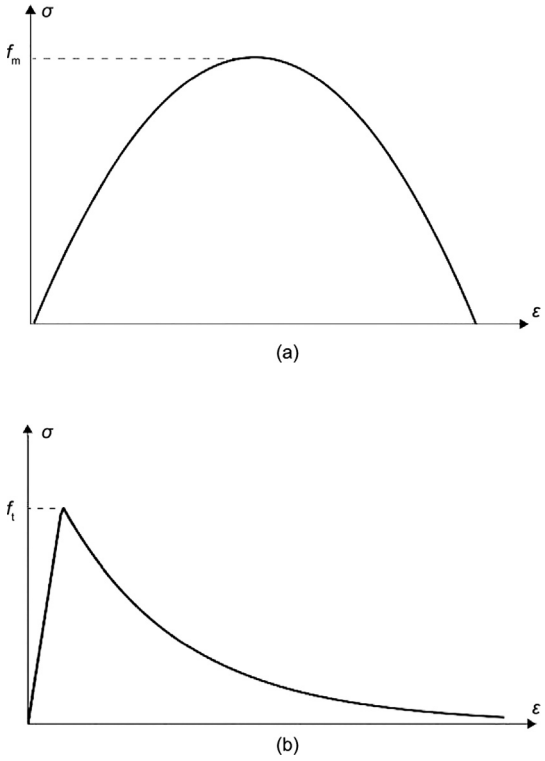

Fig. 15. Nonlinear modeling of masonry: (a) compressive behavior of masonry, where f_m is the uniaxial compressive strength, and (b) tensile behavior of masonry, where f_t is the uniaxial tensile strenth.

Table 10
Experimental results of the acceleration time history prediction for the elasto–plastic model of the four-story masonry structure.

Location	MAE	MSE	R	η_r
Floor 4	0.1986	0.2647	0.9713	19 659.40
Roof	0.3100	0.8258	0.9663	19 568.49

Table 11
Experimental results of the velocity time history prediction for the elasto–plastic model of the four-story masonry structure.

Location	MAE	MSE	R	η_r
Floor 4	0.1470	0.1333	0.9573	20 407.85
Roof	0.1951	0.2706	0.9369	19 611.45

Table 12
Experimental results of the displacement time history prediction for the elasto–plastic model of the four-story masonry structure.

Location	MAE	MSE	R	η_r
Floor 4	0.0335	0.0066	0.9979	19 785.17
Roof	0.0452	0.0135	0.9962	19 573.26

4. Ablation study and comparative experiments

4.1. Ablation study

To verify the effectiveness of the physics estimator in the proposed Phy-Seisformer model, we conducted an ablation study for the physics estimator. The acceleration response time history of

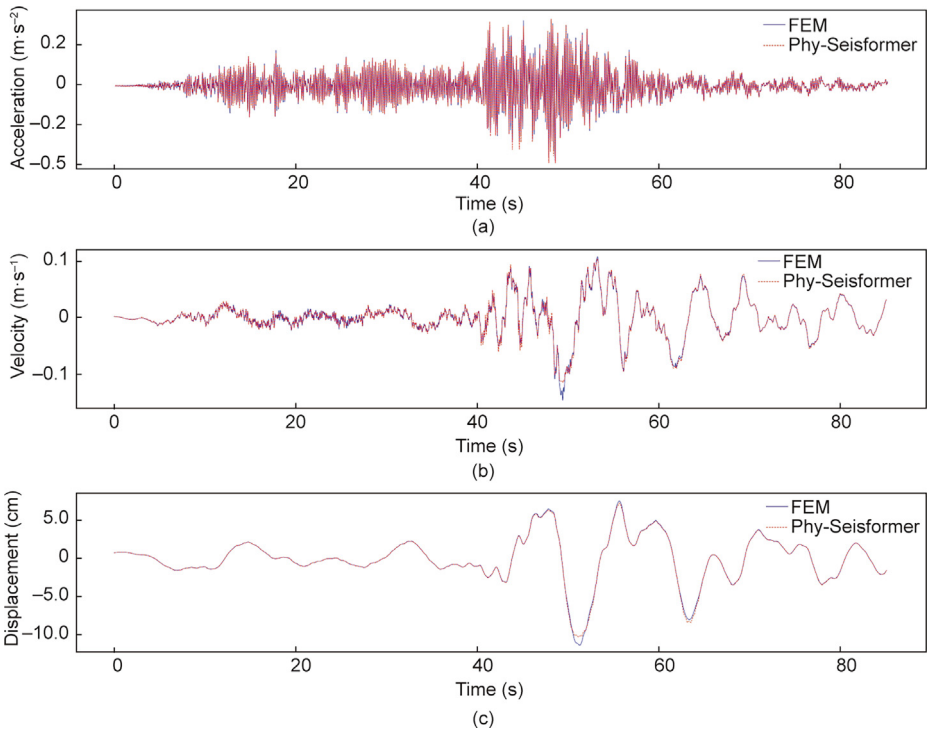

Fig. 16. Visualization of response time history prediction results for the elasto–plastic model of the four-story masonry structure.

Table 13
Experimental results of the acceleration time history prediction for the elasto–plastic model of the eleven-story irregular structure.

Location	MAE	MSE	R	η_r
Floor 4	0.3300	0.3449	0.7803	24 905.07
Floor 8	0.4792	0.6612	0.7882	24 262.07
Roof	0.7942	1.7645	0.7714	24 016.90

Table 14
Experimental results of the velocity time history prediction for the elasto–plastic model of the eleven-story irregular structure.

Location	MAE	MSE	R	η_r
Floor 4	0.2118	0.1110	0.9456	24 880.35
Floor 8	0.3743	0.3672	0.8903	24 026.83
Roof	0.5808	0.9576	0.8522	23 982.54

Table 15
Experimental results of the displacement time history prediction for the elasto–plastic model of the eleven-story irregular structure.

Location	MAE	MSE	R	η_r
Floor 4	0.0801	0.0134	0.9974	23 292.74
Floor 8	0.1643	0.0826	0.9828	21 718.29
Roof	0.2443	0.1732	0.9702	22 029.75

the roof in the eleven-story reinforced concrete irregular structure of the elasto–plastic model was selected as the dataset for the ablation experiment. The tested models were Phy-Seisformer and Phy-Seisformer without the physics estimator and the corresponding feature extraction module. The experimental results are presented in Table 19. A comparison of the prediction results of the two models under the input of the NGA06163 and NGA02646 seismic waves is shown in Fig. 19. The experimental results show that the model with the added physics estimator can fully use structural information to significantly improve the accuracy of the response time history prediction.

4.2. Comparative experiment of seismic wave amplitude

Owing to the damage and stiffness degradation of the components in the time–history analysis of the elasto–plastic model, the calculation results of the time–history analysis changed significantly with the transformation of the amplitude of the seismic wave. This experiment aimed to explore the differences in prediction accuracy under two seismic wave amplitude conditions. In the code for the seismic design of buildings [50], Shanghai falls under the seismic fortification intensity of seven degrees, which corresponds to a seismic wave amplitude of 2200 mm·s^{-2} during structure design. Therefore, in this study, the same 200 seismic waves were used to conduct comparative experiments under two amplitude ranges, 350–2200 and 350–3500 mm·s^{-2}. The dataset used the acceleration time histories of all nodes on the top floor (roof) of the eleven-story reinforced concrete irregular structure. The results of the experiment are listed in Table 20, where the two data points before and after the oblique line in each grid represent the experimental results under the two cases of seismic wave amplitude, 350–2200 and 350–3500 mm·s^{-2}, respectively. The results show that when the Phy-Seisformer model performs a time history prediction for the elasto–plastic model, the prediction results varied with changes in the seismic wave amplitude range. The prediction accuracy is relatively high when the seismic wave amplitude is small.

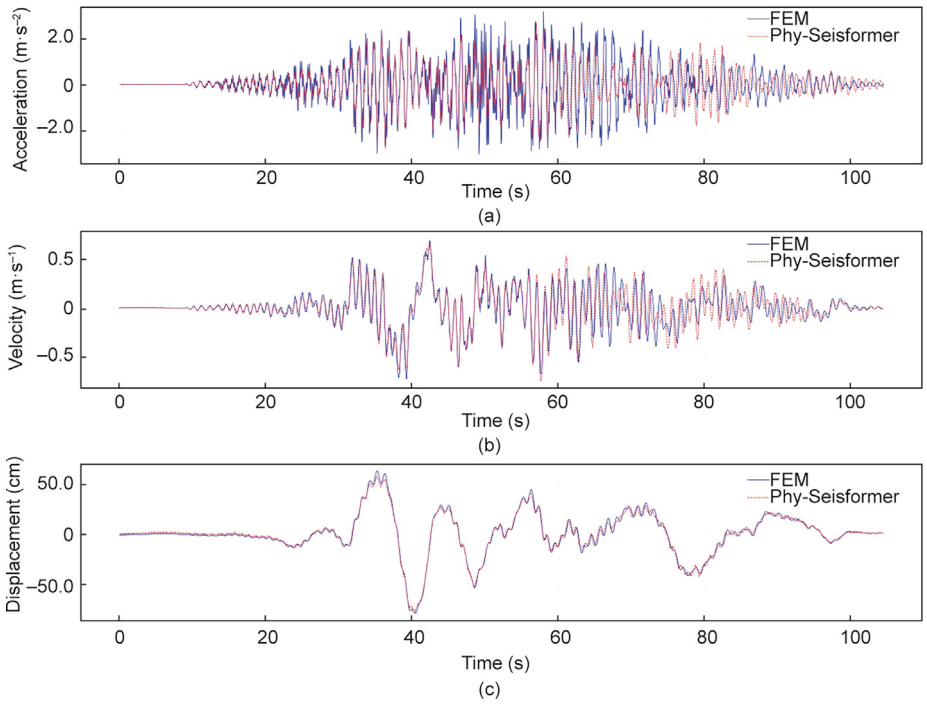

Fig. 17. Visualization of response time history prediction results for the elasto–plastic model of the eleven-story reinforced concrete irregular structure.

Table 16
Experimental results of the acceleration time history prediction for the elasto–plastic model of the twenty-one-story reinforced concrete frame structure.

Location	MAE	MSE	R	η_r
Floor 5	0.1613	0.0893	0.8890	13 619.43
Floor 10	0.1096	0.0396	0.9711	14 045.40
Floor 15	0.1362	0.0513	0.9589	14 182.30
Floor 20	0.1418	0.0596	0.9527	13 353.63
Roof	0.0956	0.0380	0.9820	13 352.81

Table 17
Experimental results of the velocity time history prediction for the elasto–plastic model of the twenty-one-story reinforced concrete frame structure.

Location	MAE	MSE	R	η_r
Floor 5	0.1888	0.0847	0.9446	14 012.95
Floor 10	0.1124	0.0408	0.9789	13 335.96
Floor 15	0.1109	0.0332	0.9858	13 473.11
Floor 20	0.1291	0.0516	0.9862	14 154.70
Roof	0.1316	0.0618	0.9883	14 118.02

Table 18
Experimental results of the displacement time history prediction for the elasto–plastic model of the twenty-one-story reinforced concrete frame structure.

Location	MAE	MSE	R	η_r
Floor 5	0.0732	0.0133	0.9948	14 266.02
Floor 10	0.1185	0.0344	0.9944	13 489.98
Floor 15	0.1272	0.0392	0.9932	14 020.40
Floor 20	0.1994	0.1026	0.9875	13 870.78
Roof	0.2323	0.1495	0.9892	13 957.52

4.3. Comparative experiment of model selection

In the field of structural response prediction, the LSTM-based model [33,34] is one of the most commonly used models and has the highest prediction accuracy in existing research. To verify the effectiveness of the Phy-Seisformer model proposed in this study compared with that of existing models, a comparison experiment was conducted. To ensure a fair comparison between Phy-Seisformer and LSTM, only the SeisBlock part of Phy-Seisformer was replaced by the LSTM model, whereas other parts of the model, including the physics estimator, remained unchanged. The LSTM model followed the same input and output as SeisBlock, adopting a sequence-to-sequence architecture identical to that presented by Meng et al. [51]. The acceleration response time history of the roof in the eleven-story reinforced concrete irregular structure of the elasto–plastic model was selected as the dataset for the comparative experiment. The experimental results are listed in Table 21. demonstrating that Phy-Seisformer outperformed the LSTM-based model significantly in building structural response prediction.

5. Discussion

This study presents a novel method for high-precision real-time response prediction of multiple nodes in building structures. By incorporating the physical information of the structures, the proposed method enables rapid and accurate structural response prediction. The effectiveness, accuracy, and computational efficiency of the proposed model were validated through a series of experiments conducted on various buildings. The effectiveness of the proposed method was validated for different types of building structures. The proposed method holds the potential for widespread application in the civil engineering domain, particularly for rapid prediction tasks related to a diverse range of building structural responses. It could provide crucial support for structural health monitoring, seismic damage assessment, and other essential aspects of building maintenance and safety. However, the method

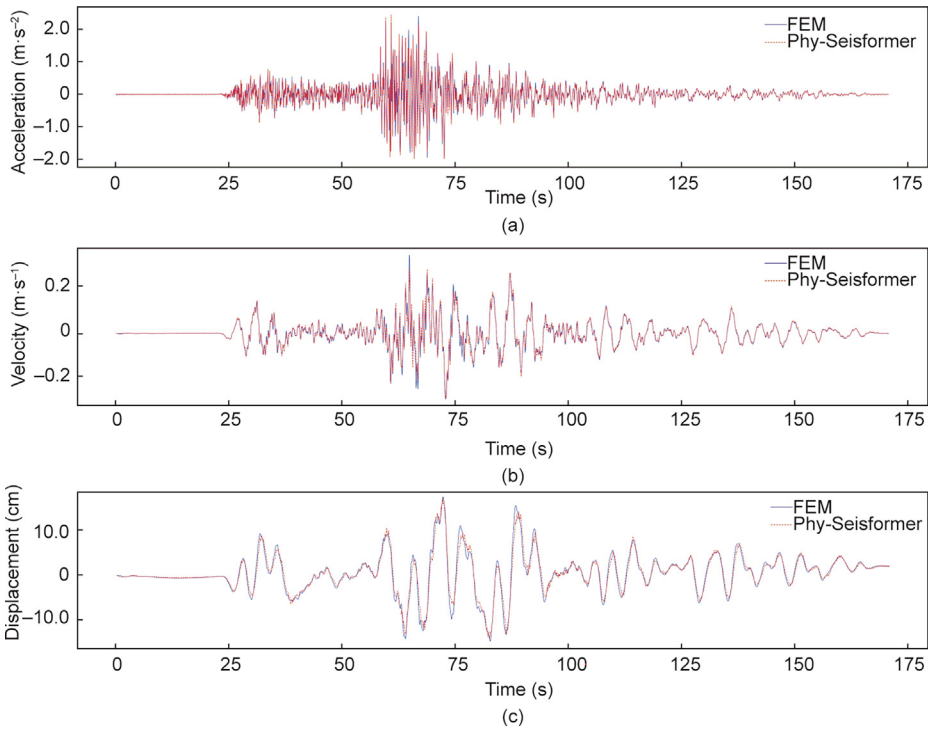

Fig. 18. Visualization of response time history prediction results for the elasto–plastic model of the twenty-one-story reinforced concrete frame structure.

Table 19
Ablation study of the physics estimator in the Phy-Seisformer.

Model	MAE	MSE	R	η_r
Phy-Seisformer (without physics estimator)	0.9486	2.2398	0.4866	51 869.25
Phy-Seisformer	0.7942	1.7645	0.7714	24 016.90

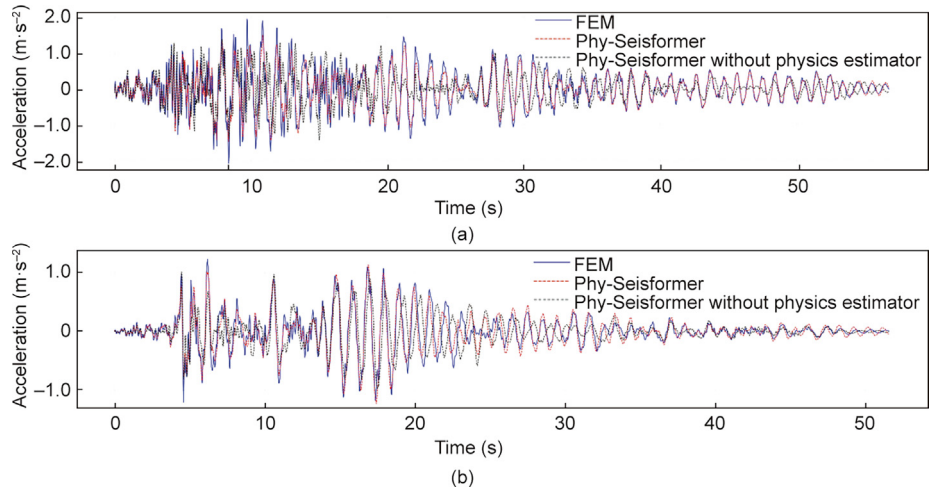

Fig. 19. Visualization of the acceleration response time history prediction results for the Phy-Seisformer model with and without the physics estimator under the input of the (a) NGA06163 and (b) NGA02646 seismic waves.

proposed in this study did not consider the spatial relationships between different nodes in the building structure. Thus, future research should explore ways to incorporate these spatial relationships to enhance the prediction accuracy of this method. In addition, the method presented in this study exhibits an important limitation regarding its applicability to cases in which the response of a building structure is so large that it collapses. However, this method does not consider a large deformation of the structure, which is a critical factor in such cases. Therefore, it cannot be utilized to analyze and predict the behavior of a building subjected to

Table 20
Comparative experiment of seismic wave amplitude.

Maximum amplitude ($mm \cdot s^{-2}$)	MAE	MSE	*R*
2200	0.7144	1.5176	0.8568
3500	0.7942	1.7645	0.7714

Table 21
Comparative experiment of model selection.

Model	MAE	MSE	*R*
LSTM	1.1740	4.0273	0.3381
Phy-Seisformer	0.7942	1.7645	0.7714

extreme loading conditions. One potential research direction that could enhance the practical applicability of the Phy-Seisformer model is to enhance its transferability between different building structures.

6. Conclusions

This study proposes a high-precision real-time structural response time history prediction method under seismic action based on deep learning and a physics estimator. The proposed method can predict the acceleration, velocity, and displacement response time histories of numerous nodes, thereby providing the necessary input for subsequent structural damage assessments. In addition, this study proposes a Phy-Seisformer model based on the Transformer model and a numerical calculation method. Structural physical information is integrated into the data-driven calculation process through a physics estimator so that the model can achieve better prediction results. Moreover, the proposed method can be easily applied to the structural response prediction of high-rise buildings. The experimental results demonstrate that the proposed method delivers consistently accurate predictions across various structures, including four-story masonry, eleven-story reinforced concrete irregular, and twenty-one-story reinforced concrete frame structures. Notably, when predicting a building's response time history in the case of elasto–plastic calculations, the Phy-Seisformer prediction speed can be at least ten thousand times faster than that of FE calculations. The effectiveness of the proposed method was validated for different types of building structures. The ablation experiment showed that the physics estimator in the Phy-Seisformer model proposed in this study can effectively use structural physical information to achieve better prediction results than a simple ground motion input. This study also investigated the impact of different amplitude ranges of the ground motion input on the prediction effect of the model. The test results indicated that the prediction accuracy of the model was better when the seismic wave amplitude was small. Future research should focus on improving the prediction effect of real-time structural response prediction for a more extensive range of seismic wave amplitudes.

Compliance with ethics guidelines

Ying Zhou, Shiqiao Meng, Yujie Lou, and Qingzhao Kong declare that they have no conflict of interest or financial conflicts to disclose.

Acknowledgments

The authors gratefully acknowledge the financial support from the Distinguished Young Scientist Fund of the National Natural Science Foundation of China (52025083), the Shanghai Social Development Science and Technology Research Project (22dz1201400), and the National Natural Science Foundation of China (U2139209). Shanghai Urban Digital Transformation Special Fund (202201033).

Appendix A. Supplementary material

Supplementary data to this article can be found online at https://doi.org/10.1016/j.eng.2023.08.011.

References

[1] Spencer Jr BF, Hoskere V, Narazaki Y. Advances in computer vision-based civil infrastructure inspection and monitoring. Engineering 2019;5(2):199–222.
[2] Baek WK, Jung HS. Precise three-dimensional deformation retrieval in large and complex deformation areas via integration of offset-based unwrapping and improved multiple-aperture SAR interferometry: application to the 2016 Kumamoto earthquake. Engineering 2020;6(8):927–35.
[3] Takagi J, Wada A. Higher performance seismic structures for advanced cities and societies. Engineering 2019;5(2):184–9.
[4] Lulić L, Ožić K, Kišiček T, Hafner I, Stepinac M. Post-earthquake damage assessment—case study of the educational building after the Zagreb earthquake. Sustainability 2021;13(11):6353.
[5] Tang A, Wen A. An intelligent simulation system for earthquake disaster assessment. Comput Geosci 2009;35(5):871–9.
[6] Bianconi F, Salachoris GP, Clementi F, Lenci S. A genetic algorithm procedure for the automatic updating of FEM based on ambient vibration tests. Sensors (Basel) 2020;20(11):3315.
[7] Ministry of Housing and Urban-Rural Development of the People's Republic of China, State Administration for Market Regulation. GB/T 38591–2020: Standard for seismic resilience assessment of buildings. Chinese standard. Beijing: Standards Press of China; 2020. Chinese.
[8] Applied Technology Council and National Earthquake Hazards Reduction Program (US). Seismic performance assessment of buildings. Report. Washington DC: Federal Emergency Management Agency (FEMA); 2012.
[9] Formisano A, Chieffo N, Milo B, Fabbrocino F. The influence of local mechanisms on large scale seismic vulnerability estimation of masonry building aggregates. In: Proceedings of the International Conference of Computational Methods in Sciences and Engineering; 2016 March 17–20; Greece, Athens. New York: American Institute of Physics (AIP) Publishing; 2016.
[10] Chieffo N, Mosoarca M, Formisano A, Apostol I. Seismic vulnerability assessment and loss estimation of an urban district of Timisoara. In: Proceedings of the Institute of Physics (IOP) Conference Series: Materials Science and Engineering; 2019 April 25–26; Tatranske Matliare, Slovakia. Bristol: IOP Publishing; 2019.
[11] Chieffo N, Formisano A, Landolfo R, Milani G. A vulnerability index based-approach for the historical centre of the city of Latronico (Potenza, Southern Italy). Eng Fail Anal 2022;136:106207.
[12] Butt F, Omenzetter P. Seismic response trends evaluation and finite element model calibration of an instrumented RC building considering soil–structure interaction and non-structural components. Eng Struct 2014;65:111–23.
[13] Fu H, He C, Chen B, editors. 9-Pflops nonlinear earthquake simulation on Sunway TaihuLight: enabling depiction of 18-Hz and 8-meter scenarios. In: Proceedings of the International Conference for High Performance Computing, Networking, Storage and Analysis; 2017 Nov 12–17; Colorado, Denver. New York: Association for Computing Machinery; 2017. p. 1–12.
[14] Zhang Y, Yan XK, Ren XD, Wang S, Wu DY, Bai BD. Parallel implementation and branch optimization of EBE-FEM based on CUDA platform. Appl Comput Electrom 2020;35(6):595–600.
[15] Reyes JC, Kalkan E, Sierra A. Fast nonlinear response history analysis. In: 16th World Conference on Earthquake Engineering; 2017 Jan 9–13; Santiago, Chile. Santiago: Asociación Chilena de Sismología e Ingeniería Antisísmica (ACHISINA); 2017.
[16] Li B, Chuang WC, Spence SM. An adaptive fast nonlinear analysis (AFNA) algorithm for rapid time history analysis. In: Proceedings of the 8th International Conference on Computational Methods in Structural Dynamics and Earthquake Engineering; 2021 Jun 27–30; Athens, Greece. European: European Community on Computational Methods in Applied Sciences (ECCOMAS); 2021.
[17] Lin X, Wang K, Zhang L, Skalomenos KA, Li D. Development of a simulation platform to model, assess and visualize the earthquake disasters in city level. In: Proceedings of the 2nd International Conference on Natural Hazards and Infrastructure; 2019 Jun 23–26; Greece, Chania. Berlin: Springer; 2019.
[18] Hori M, Ichimura T. Current state of integrated earthquake simulation for earthquake hazard and disaster. J Seismol 2008;12(2):307–21.
[19] Lu X, Guan H. Earthquake disaster simulation of civil infrastructures. Beijing: Springer and Science Press; 2017.
[20] Lin KY, Lin TK, Lin Y. Real-time seismic structural response prediction system based on support vector machine. Earthq Struct 2020;18(2):163–70.

[21] Oh BK, Glisic B, Park SW, Park HS. Neural network-based seismic response prediction model for building structures using artificial earthquakes. J Sound Vibrat 2020;468:115109.
[22] Papadrakakis M, Lagaros ND. Reliability-based structural optimization using neural networks and Monte Carlo simulation. Comput Methods Appl Math 2002;191(32):3491–507.
[23] Yang D, Yang K. Multi-step prediction of strong earthquake ground motions and seismic responses of SDOF systems based on EMD-ELM method. Soil Dyn Earthq Eng 2016;85:117–29.
[24] Sahoo DM, Chakraverty S. Functional link neural network learning for response prediction of tall shear buildings with respect to earthquake data. IEEE T Syst Man Cy-S 2017;48(1):1–10.
[25] Tezcan J, Marin-Artieda CC. Least–Square–Support–Vector–Machine–based approach to obtain displacement from measured acceleration. Adv Eng Softw 2018;115:357–62.
[26] Krizhevsky A, Sutskever I, Hinton GE. Imagenet classification with deep convolutional neural networks. Commun ACM 2017;60(6):84–90.
[27] Zaremba W, Sutskever I, Vinyals O. Recurrent neural network regularization. 2014. arXiv:1409.2329.
[28] Hochreiter S, Schmidhuber J. Long short-term memory. Neural Comput 1997;9(8):1735–80.
[29] Vaswani A, Shazeer N, Parmar N, Uszkoreit J, Jones L, Gomez AN, et al. Attention is all you need. In: Guyon I, Luxburg UV, Bengio S, Wallach H, Fergus R, Vishwanathan S, editors. Advances in neural information processing systems. Pennsylvania: Curran Associates; 2017.
[30] Kim T, Kwon OS, Song J. Response prediction of nonlinear hysteretic systems by deep neural networks. Neural Netw 2019;111:1–10.
[31] Kim T, Song J, Kwon OS. Probabilistic evaluation of seismic responses using deep learning method. Struct Saf 2020;84:101913.
[32] Wu RT, Jahanshahi MR. Deep convolutional neural network for structural dynamic response estimation and system identification. J Eng Mech 2019;145(1):04018125.
[33] Gao J, Zhang C. Structural seismic response prediction based on long short-term memory network. Earthq Resist Eng Retrofit 2020;42(3):130–6. Chinese.
[34] Zhang R, Chen Z, Chen S, Zheng J, Büyüköztürk O, Sun H. Deep long short-term memory networks for nonlinear structural seismic response prediction. Comput Struc 2019;220:55–68.
[35] Zhang R, Liu Y, Sun H. Physics-guided convolutional neural network (PhyCNN) for data-driven seismic response modeling. Eng Struct 2020;215:110704.
[36] Perez-Ramirez CA, Amezquita-Sanchez JP, Valtierra-Rodriguez M, Adeli H, Dominguez-Gonzalez A, Romero-Troncoso RJ. Recurrent neural network model with Bayesian training and mutual information for response prediction of large buildings. Eng Struct 2019;178:603–15.
[37] Peng H, Yan J, Yu Y, Luo Y. Time series estimation based on deep Learning for structural dynamic nonlinear prediction. Structures 2021;29:1016–31.
[38] Eshkevari SS, Takáč M, Pakzad SN, Jahani M. DynNet: physics-based neural architecture design for nonlinear structural response modeling and prediction. Eng Struct 2021;229:111582.
[39] Ministry of Housing and Urban-Rural Development of the People's Republic of China, China Association for Engineering Construction Standardization. GB 50009–2012: Load code for the design of building structures. Chinese standard. Beijing: China Architecture and Building Press; 2012. Chinese.
[40] Bao SH. Time–history analysis method for seismic response of high-rise building structures. In: Bao SH, editor. New high-rise building structure. Beijing: China Water and Power Press; 2013. p. 417–9.
[41] Hashamdar H, Ibrahim Z, Jameel M. Finite element analysis of nonlinear structures with Newmark method. Int J Phys Sci 2011;6(6):1395–403.
[42] Liu XJ, Du XL. MDOF system. In: Liu XJ, Du XL, editors. Dynamic of structure. Beijing: China Machine Press; 2005. p. 119–22.
[43] Zhou M, Duan N, Liu S, Shum HY. Progress in neural NLP: modeling, learning, and reasoning. Engineering 2020;6(3):275–90.
[44] Glorot X, Bordes A, Bengio Y. Deep sparse rectifier neural networks. In: Proceedings of the Fourteenth International Conference on Artificial Intelligence and Statistics; 2011 Apr 11–13; Ft. Lauderdale, FL, USA. New York: Association for Computing Machinery; 2013. p. 315–23.
[45] Shanghai Urban and Rural Construction and Transportation Commission. DGJ08–9-2013: Code for seismic design of buildings. Chinese standard. Beijing: China Architecture and Building Press; 2013. Chinese.
[46] Kingma DP, Ba J. Adam: a method for stochastic optimization. 2014. arXiv:1412.6980.
[47] Paszke A, Gross S, Massa F, Lerer A, Bradbury J, Chanan G. Pytorch: an imperative style, high-performance deep learning library. Adv Neural Inf Process Syst 2019;32:8026–37.
[48] Ministry of Housing and Urban-Rural Development of the People's Republic of China, State Administration for Market Regulation. GB 50010–2010: Code for design of concrete structures. Chinese standard. Beijing: China Architecture and Building Press; 2015. Chinese.
[49] Clementi F. Failure analysis of Apennine masonry churches severely damaged during the 2016 central Italy seismic sequence. Buildings 2021;11(2):58.
[50] Ministry of Housing and Urban-Rural Development of the People's Republic of China, State Administration for Market Regulation. GB 50011–2010: Code for seismic design of buildings. Chinese standard. Beijing: China Architecture and Building Press; 2016. Chinese.
[51] Meng S, Zhou Y, Zhang X, Lu Y. Research on real-time prediction algorithm of seismic time history response of building structures. J Build Struct 2022;43(S1):334–44. Chinese.